Converted Phase Elastic Migration Velocity Analysis

Andrey H. Shabelansky, Alison Malcolm, Mike Fehler, Xuefeng Shang and William Rodi, Earth Resources Laboratory, Massachusetts Institute of Technology*

SUMMARY

Multi-component elastic seismic data collected at large offsets have the potential to be used in seismic imaging and velocity analysis. In this study, we present an approach for converted-phase elastic-transmission migration velocity analysis with an application for VSP and micro-seismic studies. Our approach is based on the cross-correlation between converted-phase P- and S-waves propagated backward in time, and is formulated as an inverse problem with a differential semblance criterium objective function for the simultaneous update of both P- and S-wave velocity models. The merit of this approach is that it is fully data-driven and requires only one elastic backward propagation to form an image rather than the two (one forward and one backward) acoustic propagations needed for standard RTM. Moreover, as the method does not require forward propagation, it does not suffer from migration operator source aliasing when a small number of shots are used. We present a derivation of the method and test it with the synthetic Marmousi model. We also show the differences between the standard reflection offset domain common image gathers and the converted-phase image gathers that we use for model updates.

INTRODUCTION

Wave equation migration velocity analysis (WEMVA) for reflection data has been presented and discussed in many studies, e.g., Biondi and Sava (1999); Albertin et al. (2006); Shen (2004, 2012). It has been recognized that although WEMVA has lower resolution than full waveform inversion, it typically does not suffer from the cycle skipping that is inherent to full waveform inversion. On the other hand, converted-phase transmission elastic imaging, formulated as a zero lag cross correlation between P- and S-waves (both back propagated in time), has been shown to have higher resolution (Xiao and Leaney, 2010) and fewer artifacts than reflection type imaging (Shabelansky et al., 2012). The accuracy and stability of the transmission imaging methodology as well as other depth imaging methods, depend strongly on the accuracy of the velocity models (i.e. P- and S-wave speeds). Yan (2010) analyzed the behavior of the objective function for converted P to S phases for reflection-type WEMVA and showed that it appears to be convex. Because of this, we expect transmission WEMVA to also exhibit favorable properties for estimating large-scale velocity models. In addition, converted-phase imaging depends only on the back-propagated waves, and does not require forward propagation of the point source. This eliminates the need for a priori knowledge of the time excitation function and source location.

In this paper, we outline the converted phase transmission WEMVA. Our derivation follows that in Shen (2012) for reflected acoustic waves, using a differential semblance criterium in the extended offset domain common image gather (ODCIG). Specifically, we extend the derivation to elastic waves. We test the method with the Marmousi synthetic model (Versteeg and Grau, 1991), and present results for the velocity update.

CONVERTED PHASE ELASTIC WEMVA

Our derivation of converted-phase migration velocity analysis is based on one propagation of the elastic wavefield backward in time. Unlike the conventional WEMVA that uses two wave fields from two propagations (i.e., forward and backward) for cross-correlation, we obtain the two wavefields from one propagation during which we separate the P- and S-waves at each time step. Using these two wavefields we construct extended offset image gathers. Note that, although in this study we use transmitted waves, reflected waves can be used similarly.

For the sake of simplicity, we write the extended imaging condition in 2D for elastic waves as

$$I(x,h,z) \quad = \quad \int_T^0 u_p(x-h,z,t)\cdot u_s(x+h,z,t)dt, \qquad (1)$$

where h is the horizontal local offset, and u_p and u_s are the P- and S-wave displacement vector fields, respectively. The dot product operates on the x and z vector components. Note that with this imaging condition the image is formed only at non-zero offsets, as at zero offset, the converted phase transmission and reflection coefficients are zero. The separation of the P- and S-waves can be performed in different ways, (e.g., Yan (2010)). We use the Helmoholtz decomposition for the homogeneous and isotropic elastic wave equation (Aki and Richards (2002), page 64):

$$\ddot{u} = \frac{1}{\rho}(\nabla((\lambda+2\mu)\nabla\cdot u) - \nabla\times(\mu\nabla\times u)), \qquad (2)$$

where $u = u_p + u_s$. Assuming that the density ρ is homogeneous, we define model parameters as squared velocities $\hat{\alpha} = \alpha^2 = \frac{\lambda+2\mu}{\rho}$ and $\hat{\beta} = \beta^2 = \frac{\mu}{\rho}$,with which the P- and S-wavefield components become $\ddot{u}_p = \nabla\hat{\alpha}\nabla\cdot u_p$ and $\ddot{u}_s = -\nabla\times\hat{\beta}\nabla\times u_s$.

Before further continuing the derivation, we discretize the horizontal offset h and the spatial x and z domain and keep the time t continuous. We also consider I in equation 1 as a vector for any h, representing in 1D a 2D grid of x and z.

To maximize the energy around zero-offset, we use the differential semblance objective function J,

$$J = \frac{1}{2}\sum_h (hI)^\dagger (hI), \qquad (3)$$

where the superscript † refers to the transpose of a vector.

DOI http://dx.doi.org/10.1190/segam2013-1265.1

We find the gradient of the objective function with respect to the model parameter $\hat{\alpha}$ is

$$\begin{aligned}\nabla_{\hat{\alpha}} J &= \frac{\partial J}{\partial \hat{\alpha}} = \sum_h \left(\frac{\partial I}{\partial \hat{\alpha}}\right)^\dagger h^2 I = \sum_h \left(\int \frac{\partial I}{\partial u_p}\frac{\partial u_p}{\partial \hat{\alpha}} dt\right)^\dagger r \\ &= \int \left(\frac{\partial u_p}{\partial \hat{\alpha}}\right)^\dagger \left(\sum_h \left(\frac{\partial I}{\partial u_p}\right)^\dagger r\right) dt \end{aligned} \tag{4}$$

where $r = h^2 I$ is the residual image gather. Note that when the energy is focused around zero-offset, the residual gather will be equal to zero. Note also that in the expression above we assume that $\frac{\partial u_s}{\partial \hat{\alpha}} = 0$.

The right hand side of equation 4 consists of two terms:

$\sum_h \left(\frac{\partial I}{\partial u_p}\right)^\dagger r$ and $\left(\frac{\partial u_p}{\partial \hat{\alpha}}\right)^\dagger$. To calculate the first term, we differentiate equation 1 with respect to u_p and multiply by the residual gather r to obtain

$$\begin{aligned}\left(\sum_h \left(\frac{\partial I}{\partial u_p}\right)^\dagger r\right)(x,z,t) &= \sum_h u_s^\dagger(x+2h,z,t) r(x+h,h,z) \\ &= \xi_p(x,z,t), \end{aligned} \tag{5}$$

where the shifts of $2h$ and h in u_s and r, respectively, are suggested by Shen (2004, 2012); we find that they seem to keep additional information that would be lost otherwise because $r(x,h=0,z)=0$. Note also that ξ_p is the residual vector field for P waves, meaning that if α is correct and all of the energy is focused around zero offset then $\xi_p = 0$. Note also that the residual vector field ξ is constructed as a superposition: $\xi = \xi_p + \xi_s$.

To find $\left(\frac{\partial u_p}{\partial \hat{\alpha}}\right)^\dagger$ in equation 4, we consider equation 2 with any input source function f as a linear system given as

$$Lu = L(u_p + u_s) = f, \tag{6}$$

where L is a wave propagation operator defined as

$$L = \nabla(\hat{\alpha}\nabla\cdot) - \nabla\times(\hat{\beta}\nabla\times) - \partial_t^2. \tag{7}$$

By taking the derivative of equation 6 with respect to $\hat{\alpha}$ we obtain

$$\frac{\partial L}{\partial \hat{\alpha}} u + L\frac{\partial u}{\partial \hat{\alpha}} = 0. \tag{8}$$

Since we assume again that $\frac{\partial u_s}{\partial \hat{\alpha}} = 0$ we obtain,

$$\frac{\partial L}{\partial \hat{\alpha}} u + L\frac{\partial u_p}{\partial \hat{\alpha}} = 0 \tag{9}$$

or

$$\frac{\partial u_p}{\partial \hat{\alpha}} = -L^{-1}\frac{\partial L}{\partial \hat{\alpha}} u = -L^{-1}\nabla(\nabla\cdot u), \tag{10}$$

where $\frac{\partial L}{\partial \hat{\alpha}} u$ is the adjoint source.

Therefore the integrand of the right-hand side of equation 4 becomes

$$\left(\frac{\partial u_p}{\partial \hat{\alpha}}\right)^\dagger \xi_p = -u^\dagger \nabla\nabla\cdot(L^{-1})^\dagger \xi_p = -u^\dagger \nabla\nabla\cdot\eta_p, \tag{11}$$

where $\eta_p = (L^{-1})^\dagger \xi_p$ is the wavefield found from the forward propagation of the data residuals from the image points of the extended offset gather. Note that $(\nabla)^\dagger = \nabla\cdot$ and $(\nabla\cdot)^\dagger = \nabla$ (e.g., Ben-Menahem (1981), page 954).

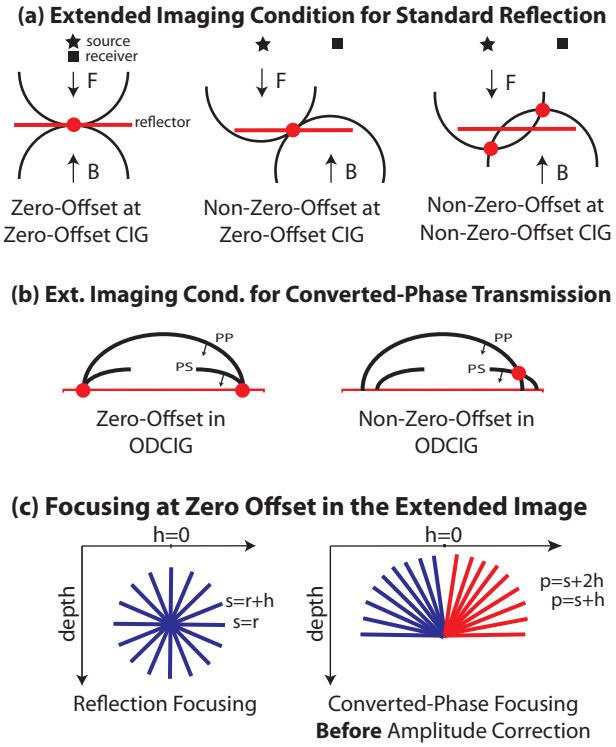

Figure 1: Schematic illustration of the extended imaging conditions for: (a) standard reflection between the forward (F) and backward (B) propagating (acoustic) wavefields; the moveout generated by the imaging condition on the left is shown for zero offset in the ODCIG and for zero-offset between the surface source and receiver. In the center, we show the zero-offset ODCIG for non-zero surface source-receiver offset. On the right, we show the non-zero offset ODCIG for non-zero surface offset. (b) converted-phase transmission waves between propagating P- and S-wavefields; the moveout shown on the left is for zero-offset in the ODCIG, on the right, the moveout is for non-zero offset in the ODCIG. (c) The summation over different moveouts for standard reflection on the left, and for converted-phase transmission on the right. The red color indicates different amplitude polarity, which is corrected by multiplying by -1 for negative offsets. The arrows on the plots define the direction of propagation, and the red dots indicate the point of interaction between different wavefields.

Thus, finally for $\nabla_{\hat{\alpha}} J$ we obtain,

$$\nabla_{\hat{\alpha}} J = \int \left(\frac{\partial u_p}{\partial \hat{\alpha}}\right)^\dagger \xi_p dt = -\int \left(u^\dagger \nabla\nabla\cdot\eta_p\right) dt. \tag{12}$$

Note that up to the derivative operators $u^\dagger\nabla\nabla\cdot\eta_p$ is a zero lag in time cross-correlation between the back-propagated data wavefield and the forward propagated residual wavefield. This is quite similar to full waveform inversion (FWI). However, the

DOI http://dx.doi.org/10.1190/segam2013-1265.1

potential advantage of this approach for micro-seismicity is the fact that we do not need to know the location and time excitation function of the micro-seismic event. Moreover, although this method has lower resolution than FWI, it does not suffer from the cycle skipping problem, inherent in FWI (Zhang et al., 2012).

Because the derivation of $\nabla_{\hat{\beta}} J$ is similar to that for $\nabla_{\hat{\alpha}} J$, we omit the former derivation and simply give the final result:

$$\nabla_{\hat{\beta}} J = \int \left(\frac{\partial u_s}{\partial \hat{\beta}} \right)^{\dagger} \xi_s dt = \int \left(u^{\dagger} \nabla \times \nabla \times \eta_s \right) dt. \qquad (13)$$

Algorithm

Each iteration of the proposed algorithm consists of the following steps:

- Propagate each elastic shot gather backward in time, and store the displacement wave fields u, u_p and u_s.
- Construct extended images I for all shots using equation 1.
- Construct residual extended image gathers r.
- Construct ξ_p and ξ_s for each shot from the stored u_p, u_s and from r.
- Calculate η_p and η_s for each shot by forward propagation.
- Construct $\nabla_{\hat{\alpha}} J$ and $\nabla_{\hat{\beta}} J$ for each shot and sum them together.
- Update model parameters $\hat{\alpha}$ and $\hat{\beta}$ using the gradients and approximated inverse Hessians, calculated by Limited Memory BFGS (Nocedal and Wright, 2000).

CONSTRUCTION OF EXTENDED IMAGES AND THE MERIT OF CONVERTED PHASE WEMVA

Conceptually, converted-phase WEMVA is very similar to standard reflection WEMVA. However, there are inherent differences between the two approaches. First, the imaging condition is based on converted phases and therefore amplitude polarity plays an important role when we construct the extended offset gathers from different propagation angles. Second, the physical construction of the extended local gathers are very different: standard reflection gathers are formed from the forward and backward propagated wavefields of the same P-wave type, whereas the converted-phase gathers are obtained from a single back-propagated elastic wavefield separated into its P and S components. Note that although here we present converted-phase WEMVA for transmitted waves, the derivation for reflection WEMVA with back-propagated converted-phase waves is similar. Figure 1 illustrates the differences between the standard and transmission approaches. Note that by shifting the wavefields, we obtain two-sided shift in offset, for reflection (Figure 1a), while for the transmission case, the shift is one-sided (i.e., the other side is zero - Figure 1b). This explains why when elastic waves propagate from different directions, they interfere with different sign. The summation over different events, shown in Figure 1c, illustrates the distribution of energy and its difference. For WEMVA we take the absolute value, and therefore we expect that the change in polarity should not affect the kinematic estimation.

PRACTICAL CONSIDERATIONS

There are many practical considerations that are unique to this WEMVA and need to be addressed. First, as mentioned above, the amplitude polarity change is generally one of the most important issues with elastic imaging and velocity analysis. Many studies address this issue and provide different solutions either correcting it in angle domain common image gathers (Lu et al., 2010) or with the help of the Poynting vector (Shang et al., 2012). However, for our synthetic study, we simply correct the amplitudes in the image domain as well as in the extended local offset domain (i.e for negative offsets we multiply the obtained image for each source by -1). The second consideration is the surface waves contained in the data that could contaminate the focusing of energy in the shallow part of the extended offset gathers. We apply a Laplacian filter on the final extended images before the residual images are constructed to reduce the effects of the surface waves. The third consideration is the fact that we need to work with vector fields. This might be cumbersome and lead to errors and instabilities. Of course, in 2D, we might work with the scalar P- and S wavefields in lieu of the vector field. However, care needs to be taken when we inject residuals for the forward propagation. The fourth consideration is the smoothing and regularization of the gradients for $\hat{\alpha}$ and $\hat{\beta}$. In our study we regularize the gradients in the so-called vertical time domain, e.g., Shabelansky (2007), which stabilizes and speeds up the convergence. The transformation for vertical time is given by

$$\begin{aligned} \nabla_{\hat{\alpha}} J(x,z) &\longrightarrow \nabla_{\hat{\alpha}} J(\tau_{\alpha}^{x}, \tau_{\alpha}^{z}) \\ \nabla_{\hat{\beta}} J(x,z) &\longrightarrow \nabla_{\hat{\beta}} J(\tau_{\beta}^{x}, \tau_{\beta}^{z}), \end{aligned} \qquad (14)$$

where vertical time τ is defined as $\tau_{\alpha}^{z} = \frac{z}{\alpha}$, $\tau_{\alpha}^{x} = \frac{x}{\alpha}$, $\tau_{\beta}^{z} = \frac{z}{\beta}$, $\tau_{\beta}^{x} = \frac{x}{\beta}$.

NUMERICAL TESTS

We test our algorithm with the Marmousi synthetic velocity model (Versteeg and Grau, 1991). This model is not only a complicated model for velocity analysis, but is also very heterogeneous, which generates many converted-phase waves that are essential for our elastic wave imaging and WEMVA. In our tests, we decompose the P-wave velocity model (Figure 2a) into the shear modulus, μ, with constant density of 2000 kg/m^3 and constant Lame parameter λ, of $4{\cdot}10^9$ Pa, and generate 22 isotropic sources equally distributed at 1200 m depth with horizontal increment of 100 m. The data are recorded with two-component receivers that are equally distributed on the surface and span the computational grid at the surface. The number of grid points in the model is $N_z = 150$ and $N_x = 287$, and the spatial increments are $\Delta x = \Delta z = 10$ m. We use a Ricker wavelet with a peak frequency of 25 Hz and Δt of 0.001 s. All elastic wave solutions, equation 2, are modeled with a 2D finite-

DOI http://dx.doi.org/10.1190/segam2013-1265.1

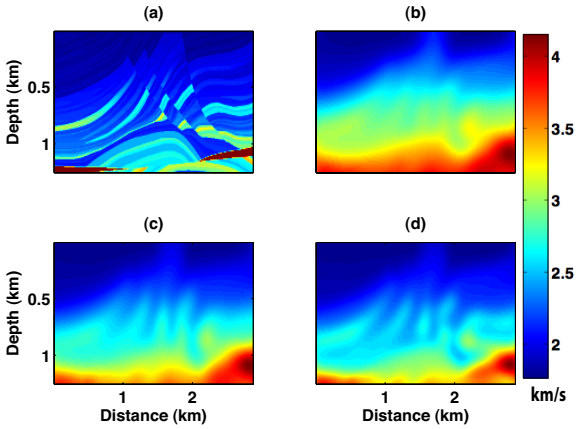

Figure 2: P-wave velocity α used for inversion: (a) true model, (b) initial model, (c) inverted model after 20 iterations, and (d) inverted model after 40 iterations.

difference solver, using a second order in time staggered-grid pseudo-spectral method with perfectly matched layer (PML) absorbing boundary conditions (Kosloff et al., 1984; Carcione, 1999; Marcinkovich and Olsen, 2003).

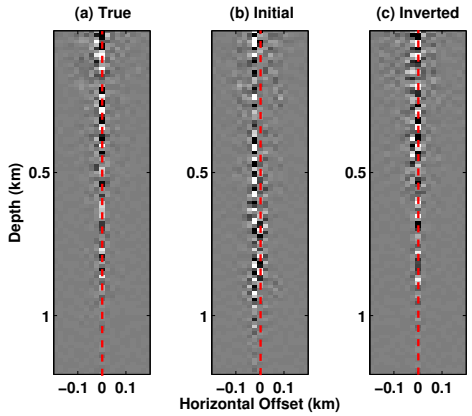

Figure 3: Transmission converted-phase ODCIG of 22 migrated shots with (a) correct velocity, (b) initial velocity and (c) inverted velocity (after 40 iterations). The horizontal position of the image gather is at 1.5 km. Note that the vertical red dashed line is positioned at $h = 0$.

Having calculated the elastic seismic data, we test our inversion with the smoothed Marmousi P-wave velocity model, shown in Figure 2b, and update only the model parameter $\hat{\alpha}$. Note that by keeping a known and constant density and λ, we update the shear modulus μ for wave propagation. For the sake of stabilization of the inversion process, we start with dh of order of three P-wave wavelengths and then after 10 iterations reduce dh to one wavelength. In Figure 2c and d, we show the results of the inversion after 20 and 40 iterations, respectively. Figure 3 shows the true, initial and inverted ODCIGs at horizontal position of 1.5 km. Note that the energy for the inverted result is focused around zero-offset.

Figure 4a shows the true reflectivity of the Marmousi model, calculated by applying a Laplacian filter to Figure 2a. Figure 4b shows the migration result using the converted-phase transmission imaging method (equation 1 with $h = 0$). This result is obtained with the correct velocity model (Figure 4a) using 22 shots. In Figure 4c, we show an equivalent migration result obtained with the initial smooth velocity model (Figure 2b), and in Figure 4d with the inverted model (Figure 2d). We observe that although the inverted result is improved, it is of a lower frequency than the image with the correct model. This effect is a subject of future investigation.

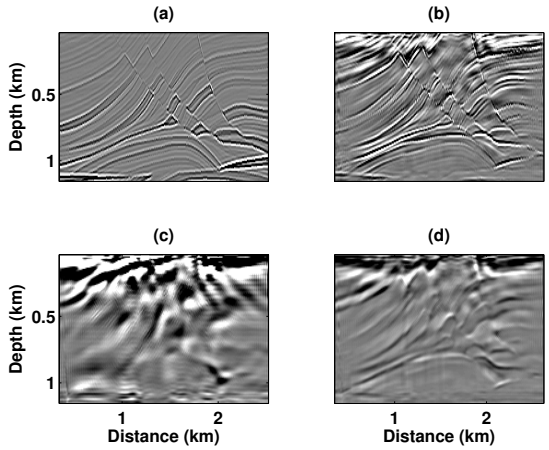

Figure 4: (a) Reflectivity model of Marmousi. Transmission converted-phase image made with 22 shots with (b) correct velocity, (c) initial velocity and (d) inverted velocity (after 40 iterations).

CONCLUSIONS

In this study we presented a data-driven method for converted phase transmission elastic migration velocity analysis. The method is formulated as an inverse problem and was tested with the Marmousi model. We were able to obtain an accurate, though low resolution, image of Marmousi from a relatively simple starting model. The results show promise for application to field data, in particular for VSP and micro-seismic applications, with a particular advantage being that it does not require forward propagation and can be applied automatically.

ACKNOWLEDGMENTS

We thank ConocoPhillips and the ERL founding members consortium at MIT for funding this work. We also acknowledge Xinding Fang and Sudhish Kumar Bakku for helpful discussion.

DOI http://dx.doi.org/10.1190/segam2013-1265.1

http://dx.doi.org/10.1190/segam2013-1265.1

EDITED REFERENCES

Note: This reference list is a copy-edited version of the reference list submitted by the author. Reference lists for the 2013 SEG Technical Program Expanded Abstracts have been copy edited so that references provided with the online metadata for each paper will achieve a high degree of linking to cited sources that appear on the Web.

REFERENCES

Aki, K., and P. G. Richards, 2002, Quantitative seismology, Theory and Methods, 2 ed.: University Science Books.

Albertin, U., P. Sava, J. Etgen, and M. Maharramov, 2006, Adjoint wave-equation velocity analysis: 76th Annual International Meeting, SEG, Expanded Abstracts, 3345–3349.

Ben-Menahem, A., and S. J. Singh, 1981, Seismic waves and sources, 2 ed.: Springer-Verlag.

Biondi, B., and P. Sava, 1999, Wave-equation migration velocity analysis: 69th Annual International Meeting, SEG, Expanded Abstracts, 1723–1726.

Carcione, J. M., 1999, Staggered mesh for the anisotropic and viscoelastic wave equation: Geophysics, **64**, 1863–1866.

Kosloff, D., M. Reshef, and D. Loewenthal, 1984, Elastic wave calculations by the Fourier method: Bulletin of the Seismological Society of America, **74**, 875–891.

Lu, R., J. Yan, P. Trynin, J. Andreson, and T. Dickens, 2010, Elastic RTM: anisotropic wave-mode separation and converted-wave polarization correction: 80th Annual International Meeting, SEG, Expanded Abstracts, 3171–3175, http://dx.doi.org/10.1190/1.1444692.

Marcinkovich, C., and K. Olsen, 2003, On the implementation of perfectly matched layers in a three-dimensional fourth-order velocity-stress finite difference scheme: Journal of Geophysical Research, **108**, no. 18, 1–16.

Nocedal, J., and S. Wright, 2000, Numerical optimization, 2 ed.: Springer-Verlag.

Shabelansky, A., 2007, Full wave inversion: Master's thesis, Tel Aviv University.

Shabelansky, A., A. Malcolm, and S. Fehler, M. Bakku, 2012, Seismic imaging of hydraulically-stimulated fractures: A numerical study of the effect of the source mechanism: 82nd Annual International Meeting, SEG, Expanded Abstracts, http://dx.doi.org/10.1190/segam2012-1182.1.

Shang, X., M. de Hoop, and R. van der Hilst, 2012, Beyond receiver functions: Passive source reverse time migration and inverse scattering of converted waves: Geophysical Research Letters, **39**, no. 15, http://dx.doi.org/10.1029/2012GL052289.

Shen, P., 2004, Wave equation migration velocity analysis by differential semblance optimization: PhD thesis, Rice University.

Shen, P., 2012, An RTM based automatic migration velocity analysis in image domain: 82nd Annual International Meeting, SEG, Expanded Abstracts, http://dx.doi.org/10.1190/segam2012-0214.1.

Versteeg, R., and G. Grau, 1991, The Marmousi experience: Proceedings of the 1990 EAGE workshop on practical aspects of seismic data inversion.

Xiao, X., and W. Leaney, Local vertical seismic profiling (VSP) elastic reverse-time migration and migration resolution: Salt-flank imaging with transmitted P-to-S waves: Geophysics, **75**, no. 2, S35–S49, http://dx.doi.org/10.1190/1.3309460.

Yan, J., 2010, Wave-mode separation for elastic imaging in transversely isotropic media: PhD thesis, Colorado School of Mines.

Zhang, Y., B. Biondi, and Y. Tang, 2012, Residual moveout-based wave-equation migration velocity analysis: 82nd Annual International Meeting, SEG, Expanded Abstracts, http://dx.doi.org/10.1190/segam2012-0332.1.